J Solid State Electrochem (2010) 14:965–973
DOI 10.1007/s10008-009-0886-2

ORIGINAL PAPER

Corrosion behavior of the steel used as a huge storage tank in seawater

Weiming Liu · Hanqian Zhang · Zhaoxia Qu · Yingqiao Zhang · Jinfu Li

Received: 12 March 2009 / Revised: 8 June 2009 / Accepted: 11 June 2009 / Published online: 11 July 2009

Abstract Open-circuit potential (OCP), polarization curve, and electrochemical impedance spectroscopy (EIS) measurement were used to investigate the corrosion behaviors of high-strength low-alloy (HSLA) steel and mild steel in seawater. Both steels were used in the construction of a huge oil storage tank. The OCP results show that the HSLA steel quickly reached more negative E_{OCP} values than the mild steel. Polarization curve results reveal that the HSLA steel exhibits higher corrosion currents and more negative corrosion potentials than the mild steel. EIS measurements reveal that both steels exhibit similar corrosion behaviors up to 144 h, one increased capacitance loop can be shown in EIS diagrams. The mild steel presents higher corrosion resistances than the HSLA steel at former stage, which is associated with the effect of the grain size. After 240 h of immersion, both steels present different corrosion behaviors. The EIS diagrams exhibit two capacitance arcs for the HSLA steel and one capacitance arc for the mild steel, which is due to the formation of intact corrosion scales on the electrode surface of the HSLA steel as to introduce a new reaction interface. The HSLA steel exhibits higher corrosion resistances than the mild steel at latter stage of experiment, which is ascribed to the synthetic actions of residual Fe_3C and the protective property of corrosion products.

W. Liu (✉) · H. Zhang · Y. Zhang · J. Li
Shanghai Jiao Tong University,
Shanghai 200240, People's Republic of China
e-mail: liuweiming1979@gmail.com

H. Zhang · Z. Qu
Baosteel Research Institute,
Shanghai 200240, People's Republic of China

Keywords Electrochemical techniques · Surface properties · EIS · HSLA steel · Mild steel

Introduction

The mild steel and high-strength low-alloy (HSLA) steel are the most commonly used construction material as a huge oil storage tank in oil and gas industry, which is due to its predominant weld property and excellent mechanical property. They are, however, very susceptible to attack in environment containing chloride. This corrosion attack takes places at the bottom of a huge oil storage tank, which makes it being eroded heavily and shortens its service life. As a result, great economic losses are caused by the corrosion of a huge oil tank. In addition, seawater is deemed to substitute freshwater in the hydraulic experiment that checks the whole strength and seal performance of a huge oil tank before it is in use. Seawater hydraulic measurement can economize lots of freshwater resources and construction costs, whereas seawater contains high density of chloride and produces serious corrosion for the HSLA steel. The detailed researches about the steels used in a huge oil storage tank in seawater are very few. Thus, it is necessary to study the corrosion processes of both steels in seawater.

As well known, the grain size and microstructure in materials greatly affect their corrosion performance. Di Schino and Kenny [1, 2] investigated the effect of highly refined grain size on the corrosion behavior of AISI 304 steel and disclosed certain improvements in the intergranular and pitting corrosion resistance due to micron-scale grain sizes. These various microstructural components (ferrite, perlite, bainite, martensite) could influence not only the mechanical property but also the corrosion

resistance of the material [3]. The corrosion performance of the steel was related to the shape of Fe_3C in microstructure. The reason for this is that Fe_3C is part of the original steel in the nonoxidized state that accumulates on the surface after the preferential dissolution of ferrite (*a*-Fe) [4]. It is suggested that cementite provides an available area for the cathodic reactions [5, 6]. Zhang CL et al. [7] had reported that pearlite in weathering steel 09CuPCrNi deteriorated its corrosion resistance. Zhao Y T found that low-alloy steel showed improved corrosion resistance than weathering steel, which was due to suppression of the formation of pearlite [8]. However, the corrosion behavior of the HSLA steel with bainite still remains poorly understood.

Generally, the corrosion behavior of steel is largely controlled by the presence or absence of a protective oxide film, which may act as a protective barrier layer against corrosion attacks. Therefore, the corrosion resistance of steel is closely related to its electron property. As reported in literatures, electronic properties of a passive film were expected to be of crucial importance in understanding their protective characters against corrosion [9–11]. Since film dissolution, formation, and breakdown are involved in the movement of the electrons and ions, electron properties represent one of the most significant features of a passive film with respect to its corrosion resistance [12] and which may play an important role in film breakdown mechanisms.

Based on this, the purpose of this work was devoted to study the corrosion process of the HSLA steel with bainite and mild steel with pearlite used as a huge oil tank in seawater. The electrochemical methods were used to characterize the corrosion behaviors of both steels in seawater, particularly by the electrochemical impedance method.

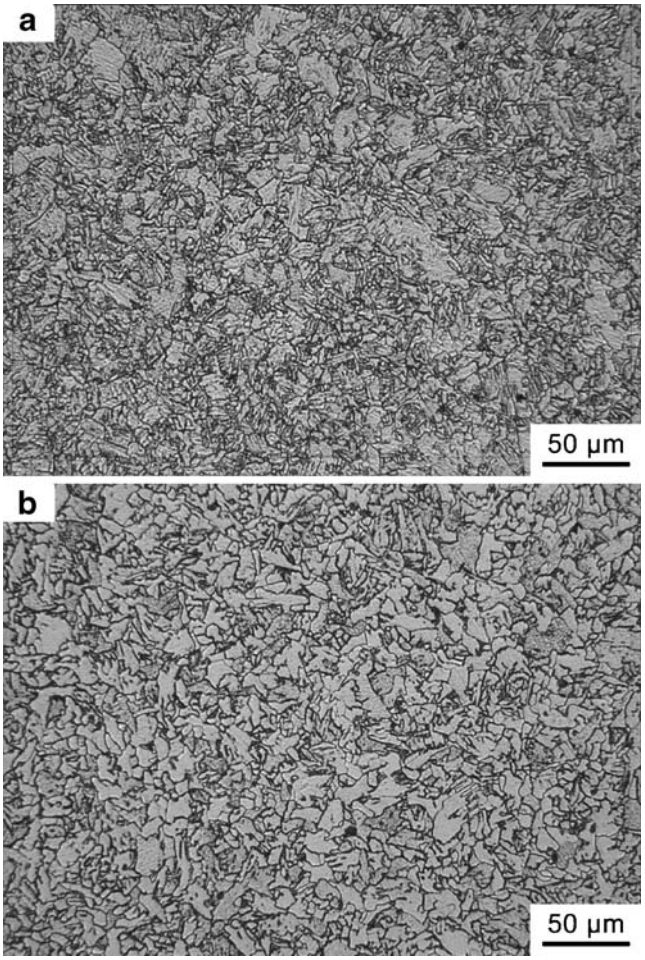

Fig. 1 Microstructure of samples: **a** HSLA steel, **b** mild steel

Experiments

The materials used for tests were the HSLA steel and mild steel used in a huge oil storage tank, in which compositions were given in Table 1. The microstructure of the HSLA steel is bainite and that of the mild steel is pearlite, as shown in Fig. 1. It can be shown that the mild steel exhibits much larger grain sizes than the HSLA steel. Every electrode specimen was a disk with a surface area of 1 cm^2, attached to a copper wire to the rear face. Every surface was embedded in epoxy resins, leaving a working surface of 1 cm^2. The polishing methods used to prepare sample surface were as follows: first, the electrode surface was polished with emery paper (grade 400) and distilled water. The surface was then polished with emery paper (grade 600) until a homogeneous surface was obtained and then rinsed with acetone. Finally, a specimen was subjected for 5 min to ultrasonic washing with acetone and dried in warm flowing air prior to every experiment. Electrochemical impedance spectroscopy (EIS) and polarization curve began after an initial delay of 2 h for samples to reach a steady-state condition.

Experimental device description

All the electrochemical measurements were performed in a standard three electrochemical cells, with a saturated

Table 1 Chemical composition of the HSLA steel and mild steel (wt.%)

Composition Specimen	C	Si	Al	Mo	Cr	Cu	Nb	Ni	S	P
HSLA steel	0.090	0.185	0.032	0.2	0.03	0.01	0.014	0.21	0.0015	0.0043
Carbon steel	0.139	0.299	0.034	–	0.02	–	0.017	0.02	0.004	0.0118

calomel electrode as the reference electrode, a platinum sheet as the auxiliary electrode, and the samples as the working electrode. Open-circuit potential (OCP), polarization curve, and EIS test were carried out in a VMP3 electrochemical corrosion testing apparatus under room temperature in seawater. Open-circuit potential measurement immediately began after the specimens were immersed in seawater and taken every 10 min. For the potentiodynamic curve, the sweeping potential was from −0.25 to 0.25 V with a scanning rate of 0.1667 mV/s. All impedance measurements were performed at the open-circuit potential with alternating current amplitude of 5 mV. The applied frequencies ranged from 0.01 Hz to 10 kHz. At least three tests were conducted for each condition to confirm the validity of the experiment measurements.

Surface characteristic

Scanning electrode microscopy (SEM) was utilized to investigate the morphology of covered and removed corrosion scales for the HSLA steel and mild steel by SEM analyses after 720 h of immersion in seawater. The microstructure of the corrosion scales were analyzed using X-ray diffractometer conducted by using a Rigaku diffractometer with Cu Kα radiation.

Results and discussion

Surface character

Surface characters are shown in Fig. 2 for SEM analyses after 720-h immersion in seawater; every steel sample was taken out from the electrochemical cell, dried with N_2 gas flow, and left in a dryer. SEM images show that the corrosion scales of both steels present two layers. The two layers exhibit an inner rust layer with adherent characteristic and an outer rust layer is less adherent than an inner rust layer. It can be seen that the protective ability of corrosion scales depends on the performance of the inner rust layer. Obviously, it can be shown in Fig. 2a for the morphology of corrosion scales for the HSLA steel that the intact outer rust layer with some cracks are tightly combined with the inner rust layer. However, the corrosion scales for the mild steel show that the cracked outer layer loosely covers over the inner rust layer, as shown in Fig. 2b. This discloses that the corrosion scales of the HSLA steel exhibit better protective property in seawater. The compositions of the corrosion scales measured by X-ray diffraction are shown in Fig. 3. It shows that the corrosion scales of specimens are all principally composed of the corrosion substance in seawater (NaCl), corrosion products (α-FeOOH, γ-FeOOH, Fe_3O_4, Fe_2O_3), and residual cementite (Fe_3C).

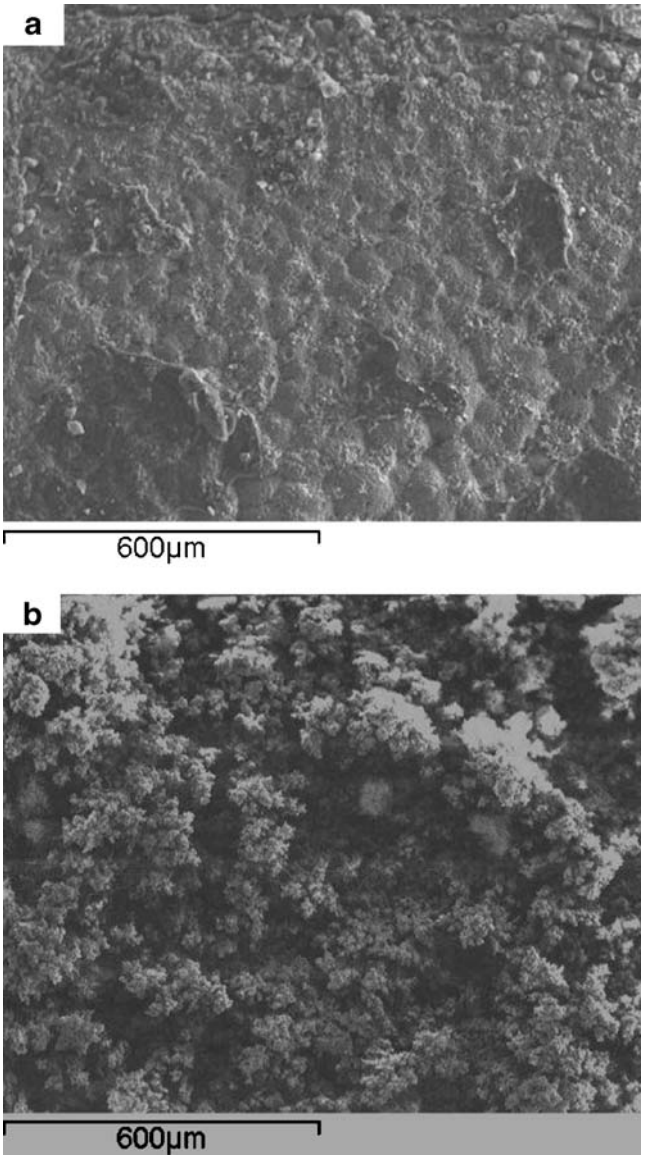

Fig. 2 SEM micrographs of corrosion scales in seawater: **a** HSLA steel, **b** mild steel

Figure 4 shows SEM images of all samples where corrosion scales were removed after 720 h of immersion in seawater. Every sample was rid of the corrosion scales in HCl + $C_6H_{12}N_4$ solution by proportion and dried with N_2(g) flow and left in a desiccator. It can be shown that some local holes and many residual Fe_3C appear on electrode surface. This indicates that local corrosion took place on the electrode surface. The mild steel sample (Fig. 4b) shows rougher surface and more magnitudes of Fe_3C remainders than the HSLA steel (Fig. 4a), which indicates that the mild steel suffers serious corrosion in seawater.

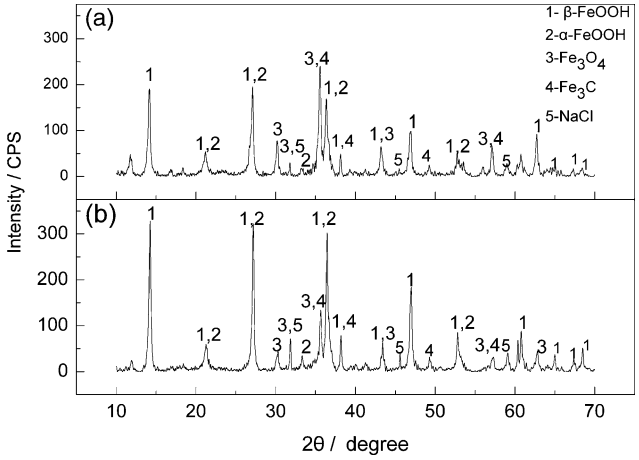

Fig. 3 X-ray diffraction of corrosion scales: *a* HSLA steel, *b* mild steel

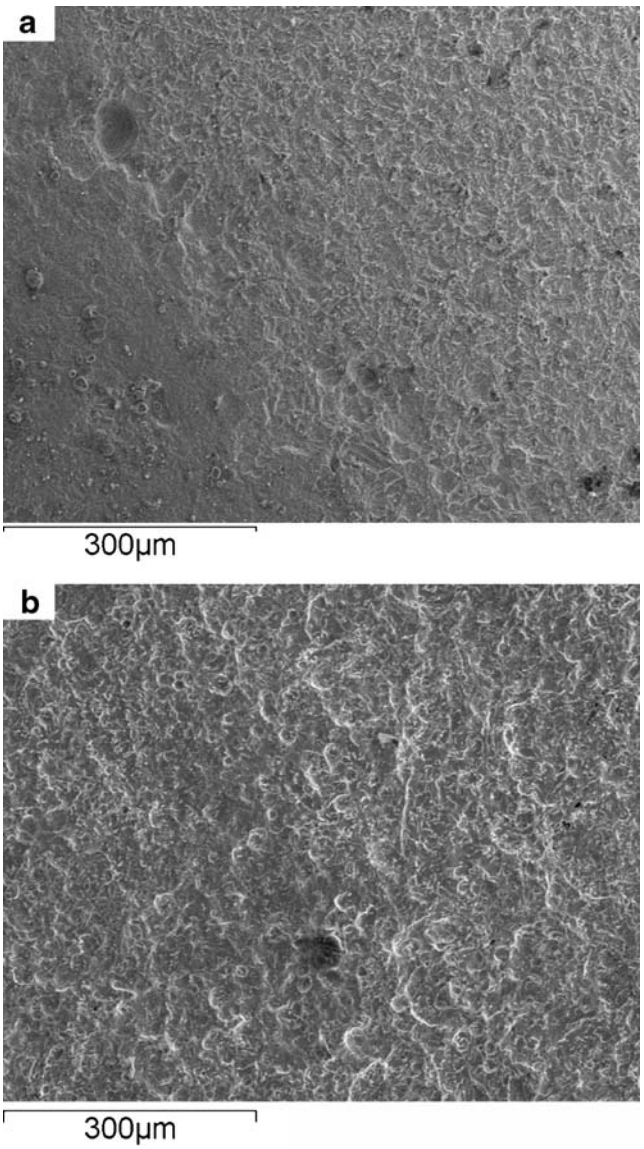

Fig. 4 SEM micrographs of removed scales: **a** HSLA steel, **b** mild steel

Open corrosion potential measurement

The evolution of OCP with times for the HSLA steel and the mild steel after 16 h of immersion in seawater was illustrated in Fig. 5. It can be shown that corrosion potentials of both steels approach relatively stable values after 2 h of immersion, and the HSLA steel shows more negative shift in OCP values compared with the mild steel, which is due to its smaller grain sizes and more magnitudes of precipitation phases in microstructure of the HSLA steel. It is well known that the grain boundaries are regions of preferable attack sites when exposed to a corrosion environment [13]. Therefore, the detrimental preferential grain attack is largely increased for the HSLA steel due to high fractions of grain boundaries on its reaction interface. In addition, the precipitation phase is sites of a cathodic reaction zone. Therefore, the HSLA steel shows quicker decrease in OCP. The initial gradual decrease in corrosion potentials can be attributed to the dissolution of the air-formed corrosion scales on the electrode surface [14]. In addition, it can be shown that it is unreliable to perform electrochemical measurements immediately after immersion since the electrode is still in a transition state.

Polarization curve

The polarization curves of the HSLA steel and the mild steel in seawater can be illustrated in Fig. 6. In general, the anodic current density continuously increases with an increase in corrosion potential. This indicates that both steels demonstrate active dissolution behavior in seawater. It can be shown that the HSLA steel shows higher corrosion currents and more negative shift in corrosion potentials when compared with the mild steel, which indicates that the mild steel shows improved corrosion resistance than the

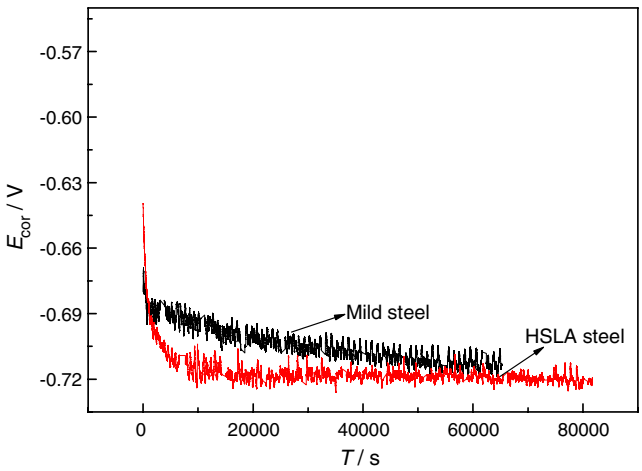

Fig. 5 Evolutions of E_{corr} with times of mild steel and HSLA steel in seawater

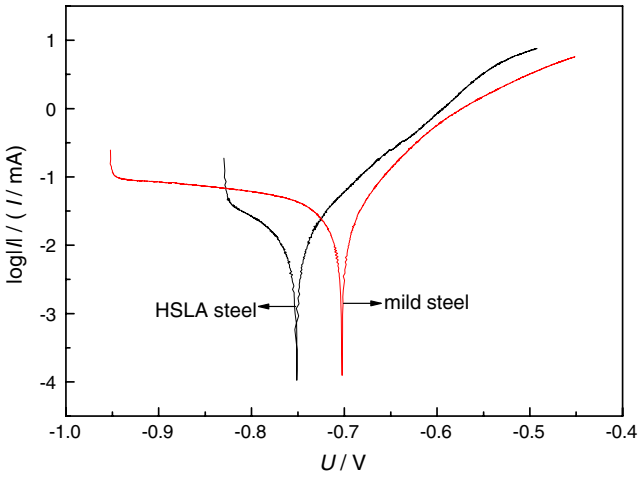

Fig. 6 Polarization curves of the HSLA steel and mild steel in seawater

HSLA steel. This behavior is associated with the synthetic effects of the grain size and microstructure. As well known, the grain boundaries are the region of preferable corrosion attack because of the residual stress caused by plastic deformation in the boundaries during growth and high activity introduced by more crystal defects (such as dislocation, cavity, and lattice distortion) and more disordered atomic arrangement. As can be seen in Fig. 1, the HSLA steel exhibits a smaller grain size. Therefore, it contains a large number of activated sites and accelerates corrosion by forming much more microelectrochemical cells between the large amount of grain boundaries and the matrix by increasing the electrochemical reactivity during corrosion process. Therefore, the HSLA steel exhibits a higher corrosion rate in seawater. This is in agreement with the results of the E_{OCP} measurement.

Electrochemical impedance spectra

The key aim of the EIS experiment is to provide insight into the characteristics and kinetics of electrochemical process occurring at the Fe/solution interface in seawater. Based on OCP results, the working electrodes had been immersed in seawater until a stable state formed. Figures 7 and 8 illustrate the typical Nyquist and Bode diagrams of the HSLA steel and mild steel obtained at different immersion times. It can be shown that both steels exhibit similar corrosion behaviors at initial stage of experiment, and the Nyquist plots of both steels show increasing capacitance arcs in Figs. 7a and 8a, indicating an activation-like behavior with a phase angle magnitude around 65°; in Figs. 7b and 8b, there is a magnitude increases over time that reaches the maximum magnitude of phase angle during the first day of immersion. This is attributed to the formation of the outer rust layer. EIS shows

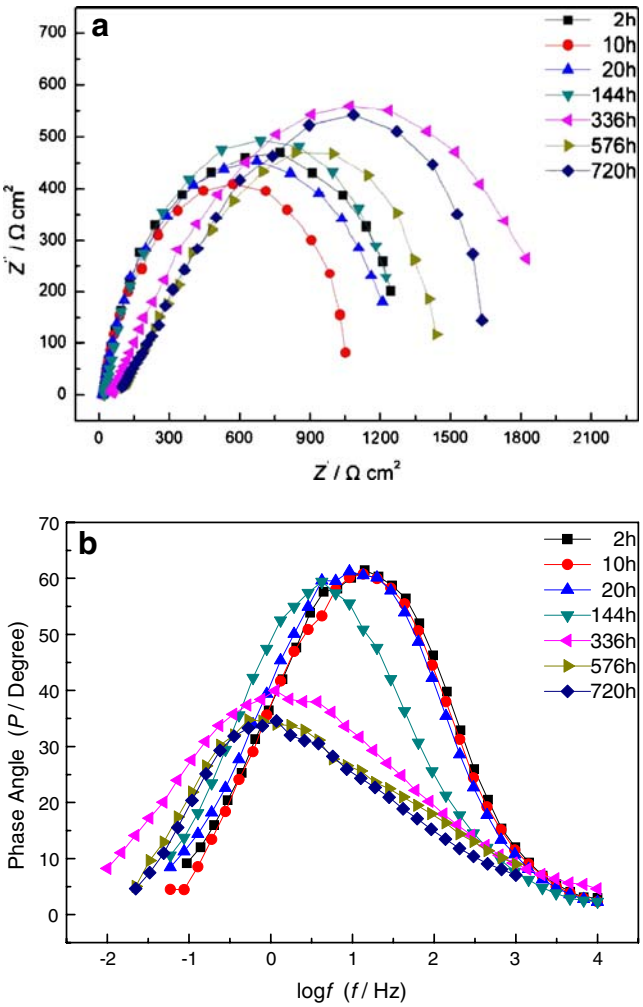

Fig. 7 Impedance spectra of HSLA steel in seawater: **a** Nyquist plots, **b** Bode plots

an increased trend with increasing times and present diffuse-like behavior up to 144 h of immersion, which indicates the formation of the inner rust layer. After 336 h of immersion in seawater, the Nyquist plots of the HSLA steel show that another capacitive loop appears at the middle frequency range. This time constant is due to the formation of stable corrosion scales on the electrode surface, as shown in Fig. 2a, which is sufficient to cover over its whole electrode surface after a long-time immersion so as to introduce a second interfacial electron exchange reaction. However, the impedance spectra for the mild steel still exhibit a simple capacitance arc. The reasons for this are that the mild steel cannot form stable protective films on its surface after a long time of immersion, as shown in Fig. 2b, and its corrosion scales are porous and loose and do not sufficiently cover its steel surface.

According to the EIS in Figs. 7 and 8, the equivalent circuits are illustrated in Fig. 9. Figure 9a is fitted to the

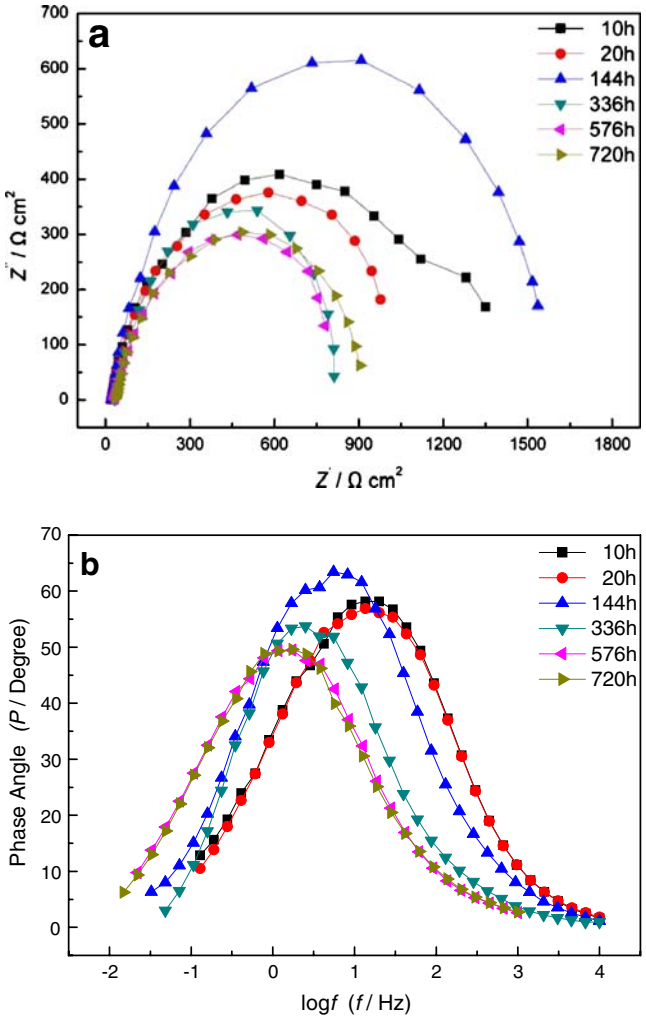

Fig. 8 Impedance spectra of mild steel in seawater: **a** Nyquist plots, **b** Bode plots

impedance spectra with one time constant and Fig. 9b is simulated to the impedance spectra with two time constants. The agreement between experimental and simulated results indicates that the experimental results are well fitted to the proposed equivalent circuits. The fitting quality was evaluated by chi-squared (χ^2) values of about 10^{-4}, as shown in Tables 2 and 3; in these models, R_s is the solution resistance; CPE_f and R_f correspond to the corrosion film capacitance and resistance, respectively. R_{ct} is the reaction resistance. CPE_{dl} is the double-layer capacitance. A constant-phase element representing a shift from an ideal capacitor was used instead of the capacitance itself for simplicity. The impedance of a constant-phase element is defined as $Z_{CPE}=[Q\ (j\omega)\ ^n]^{-1}$ [15–17], where Q is a proportional factor; ω is the frequency and $-1\leq n\leq 1$. The value of n seems to be associated with the nonuniform distribution of current as a result of roughness and surface defect.

Tables 2 and 3 show the representative parameter values of the best fit to experimental data in Figs. 7 and 8. The fitting results show that the proportional factor Q_{dl} of CPE_{dl} increases with times for both steels during corrosion process. According to Turgoose et al. [18], this increase in the capacitance Q_{dl} values is associated with an increased double-layer capacitance due to an increase in the surface area available for cathodic reaction, which is related to the electrochemical activity of nonoxidized cementite (Fe_3C) residues exposed during corrosion process. In addition, this would lead to a decrease in R_p values with time (higher corrosion rates), in contrast to the results obtained in this work, which presents a rising tendency through time for these values. To explain this behavior, an important aspect of this process must be considered. When corrosion reactions take place, the area of Fe_3C exposure increases for the mild steel. This is because the dissolution of the surrounding ferrite from the pearlite leaves a laminar structure of nonoxidized Fe_3C as shown in Fig. 4b. This

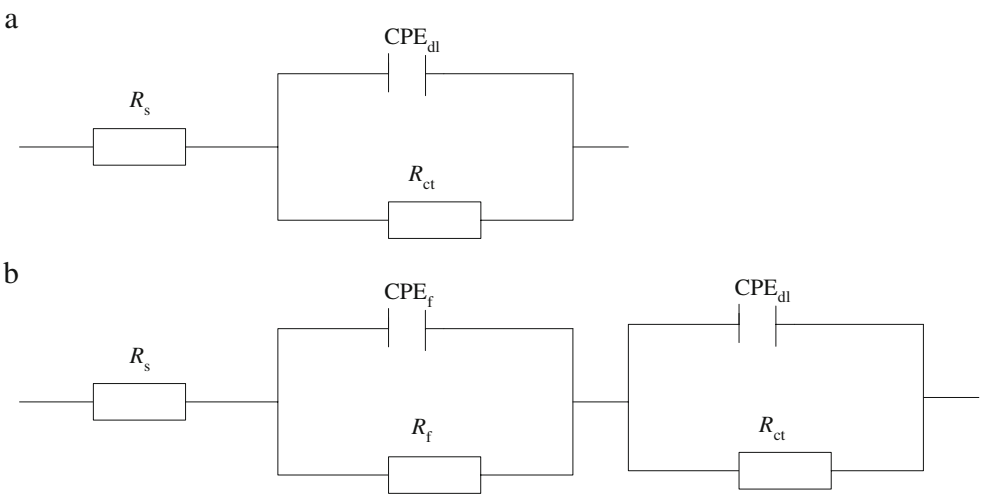

Fig. 9 Equivalent circuits used to fit experimental data of EIS diagrams for HSLA steel and mild steel in seawater

Table 2 Electrochemical parameters obtained from the HSLA steel in seawater

Time (h)	R_s (Ω cm^2)	Q_{dl} (Ω^{-1} cm^{-2} s^n)	n_{dl}	R_{ct} (Ω cm^2)	Q_f (Ω^{-1} cm^{-2} s^n)	n_f	R_f (Ω cm^2)	Q_W (Ω^{-1} cm^{-2} s^n)
2	17.75	1.95×10^{-4}	0.80	1,305				
10	17.48	2.09×10^{-4}	0.82	1,088				
20	17.13	2.49×10^{-4}	0.81	1,299				
144	23.73	4.35×10^{-4}	0.79	1,391				
336	48.2	2.80×10^{-3}	0.37	439.1	8.14×10^{-4}	0.70	1,582	0.039
576	81.6	7.70×10^{-4}	0.46	523.7	7.90×10^{-4}	0.87	1,148	
720	91.04	7.98×10^{-4}	0.65	408.1	7.98×10^{-4}	0.87	1,007	

is not removed from the sample surface. Thus, an increase in Q_{dl} values decreases for the mild steel during corrosion process. In case of the HSLA steel, of which microstructure is bainite and the grain of Fe_3C is small. When the surrounding ferrite is dissolved, the small Fe_3C phase is easy to detach from the metal surface and leave few Fe_3C residues on electrode surface, which can be shown in Fig. 4a. Therefore, the cathodic areas remain steady for the HSLA steel. As a result, The Q_{dl} values of the HSLA steel are lower than those of the mild steel in seawater. In addition, corrosion products formed on electrode surface can provide some protection to the metal beneath them by restricting the mass transfer of reactants and products between the bulk solution and the metal. Consequently, an increase in the capacitance values (Q_{dl}) could be related to the growing area of corrosion products over the surface of samples

It is well recognized that the polarization resistance (R_p) is inversely proportional to the corrosion rate. The R_p value is equal to R_{ct} value in the first 144 h and the sum of R_{ct} and R_f values after 336 h of immersion. The R_p values obtained by analyzing impedance spectra were presented in Tables 2 and 3. It can be shown that R_p values increased with times in the first 144 h, which is due to the formation of corrosion products. At the end of experiment, the decreased R_p values can be ascribed to the detachment of corrosion products. The HLSA steel presents lower R_p values compared with the mild steel at the former experiment, which is associated with the effect of the grain size in microstructure. It is well known that the grain boundaries are regions of preferable corrosion sites in corrosion medium. This is due to the electron work function decreasing at the grain boundary, which indicates that, at grain boundary, electrons are more active [19, 20]. As a result, the surface becomes more reactive in aggressive environment. In addition, as can be seen in Fig. 1, the HSLA steel has a smaller grain size compared with the mild steel. Therefore, it contains a number of grain boundaries and triple junctions which are all active sites for corrosion attack especially in seawater. As a result, preferential corrosion at grain boundaries greatly accelerates the corrosion rate of the HSLA steel. After 144 h of immersion, the HSLA steel exhibits higher magnitudes of R_p compared with the mild steel. It is believed that the smaller grain sizes and high density of grain boundaries will certainly provide a higher number of actives sites to quickly form a protective passive layer [21]. Besides, the passive film seems to be a dominating factor for the corrosion characterization, which reflects that the fine structure materials can provide the positive effect on the corrosion behavior. For this reason, it can increase adhesion strength between the passive film and substrate because of the enhancement in the electron activity at grain boundaries and possible pegging of the passive layer into grain boundaries [19, 20]. As discussed above, the increased magnitudes of residual Fe_3C can increase the corrosion rate by the increased area of cathodic reaction zone, of which phenomenon obviously plays a role on the electrode surface of the mild steel. In addition, a smaller grain size promotes the element diffusion to benefit the formation of compact passive films, which obviously enhances the corrosion resistance of material and produces uniform element distribution. As a result, these effects can

Table 3 Electrochemical parameters obtained from the mild steel in freshwater

Time (h)	R_s (Ω cm^2)	Q_{dl} (Ω^{-1} cm^{-2} s^n)	n_{dl}	R_{ct} (Ω cm^2)	Q_W (Ω^{-1} cm^{-2} s^n)
10	19.5	2.2×10^{-4}	0.79	1,299	
20	19.31	2.2×10^{-4}	0.79	1,068	
144	21.38	2.78×10^{-4}	0.83	1,575	0.069
336	34.48	4.97×10^{-4}	0.84	855.4	
576	32.45	1.11×10^{-3}	0.76	867.7	
720	33.8	1.12×10^{-3}	0.77	908.6	

decrease the amount of chloride ions adsorbed on the surface of samples and inhibit the incorporation of chloride ions into the oxide film [22]. Thus, the HSLA steel can form compact oxide scales (Fig. 2a) and impede the chloride ions' diffusion in corrosion scales. However, the corrosion scales of the mild steel are porous and loose, as shown in Fig. 2b, which leads to the seawater easily arriving to the reaction interface. Consequently, the HSLA steel presents lower corrosion rates at the end of experiment.

The porosity rate of oxide film

When a steady rust layer forms during corrosion, mass transfer process appears in the electrode impedance of low frequency. The corresponding impedance dispersion can be expressed as semi-infinite Warburg diffusion impedance connected with of diffusion of dissolved oxygen from solution to the electrode surface:

$$Z_w = \frac{\sigma}{\sqrt{\omega}} - j\frac{\sigma}{\sqrt{\omega}} = \frac{\sigma}{\sqrt{\omega}}(1-j) = \frac{\sqrt{2}\sigma}{\sqrt{j\omega}} \quad (1)$$

Where Z_w is the Warburg diffusion impedance and σ is the Warburg coefficient, which in case of a surplus of one component in redox system is often presented as

$$\sigma = \frac{RT}{z^2F^2A\sqrt{2}c\sqrt{D}} \quad (2)$$

Where c is the solution concentration of a reaction species, F=96,485 C mol^{-1} the Faraday constant, and R= 8.314 mol^{-1} K^{-1} the molar gas constant; D is the ion diffusion coefficient in corrosion scales; A is the area of working electrode. From Eq. 2 follows that the type of Z_w dispersion is formally identical with that of Z_{CPE} for n= 0.5 and Warburg coefficient can be related with CPE coefficient:

$$\sigma = \frac{1}{Q_w\sqrt{2}} \quad (3)$$

Where Q_w is the coefficient of a constant-phase element used for the description of diffusion impedance and formally substituting Z_w in equivalent circuits used for data fitting. In seawater, n_w is near to the theoretical values of 0.5 for the major part of the experiment. Its gradual increase in time up to ~0.7 was observed after a long immersion time, which should be ascribe to the surface modification due to external oxide dispersion and dissolution reaction and consequent increase of the surface roughness.

In seawater, the corrosion rate mainly depends on the oxygen concentration. After the surface oxide films formed and the corrosion rate stabilized, it was possible to measure impedance down to very low frequencies. Therefore, the protective property of oxide films can be expressed by the magnitude of D in oxide films after the formation of steady oxygen films. Using Eq. 2, the values of oxygen in corrosion scales can be calculated to be 3.14×10^{-11} m^2 s^{-1} for the mild steel and 1.02×10^{-10} m^2 s^{-1} for the HSLA steel, respectively, which indicates that the corrosion scales of HSLA steel show better protective ability than the mild steel. This is fitted to the results of EIS.

Under this experimental condition, oxygen diffusion coefficients in seawater are estimated from Einstein–Stoke equation [23]:

$$D = \frac{RT}{6\pi\eta N_A r_{o_2}} \quad (4)$$

Where R is the gas constant, T represents the absolution temperature; η is the dynamic viscosity of seawater (1.045×10^{-3} Pa S) at 20 °C; N_A is Avogadro number (6.02×10^{23}), and r_{O2} is the oxygen diameter (here is the magnitude of 1.09×10^{-10} m). It can be concluded that D values of oxygen are about 1.89×10^{-9} m^2 s^{-1} in seawater by Stokes–Einstein equation. Compared with the results of oxygen diffusion coefficient in corrosion scales, it can be shown that its value is much lower than the magnitude of the oxygen diffusion efficient in solution. Thus, the formation of corrosion scales can protect the steel matrix and slow down the corrosion rate. As well known, the ion diffusion coefficient in corrosion scales depends on the porosity of corrosion scales and is in inverse proportion to the porosity-to-tortuosity ratio, which can be expressed as follows [24]:

$$D = D_0\frac{\varepsilon}{\beta^2} \quad (5)$$

Where D_0 is the diffusion coefficient in solution; D is the diffusion coefficient in corrosion scales; ε is the porosity of corrosion scales, and β is porosity-to-tortuosity rate, which usually is $\sqrt{3}$ to the materials composed of corrosion scales. The ε values of mild steel and HSLA steel can be calculated approximately to be 4.98×10^{-2} and 1.62×10^{-1}, respectively. The calculating results verify the high porosity of corrosion scales of mild steel indicated the bad protective ability of its corrosion scales, in agreement with the EIS results.

Conclusions

The electrochemical techniques used in this investigation led to the following conclusions:

1. E_{OCP} attains to relative steady values about approximately −0.66 to −0.68 V for the HSLA steel or

approximately −0.56 to −0.58 V for the mild steel after 2 h of immersion.

2. Polarization results show that the HSLA steel shows more negative shift in corrosion potentials and higher corrosion currents compared than the mild steel, in agreement with the result of E_{corr}.
3. The interface characterization was performed by electrochemical impedance spectra of the HSLA steel and the mild steel in seawater. Analyses of EIS results show the separation of oxide layers and double-layer capacitances for the HSLA steel and combination of them for the mild steel after a long immersion time. Therefore, different equivalents circuits can be used to simulate the corrosion behaviors of both steels.
4. The mild steel shows better corrosion resistances than the HSLA steel at the earlier stage, which is due to the effect of the grain size, whereas the HSLA steel presents more improved corrosion resistances than the mild steel at the latter stage owing to the synthetic effects of the protective property of corrosion scales and the increased area of Fe_3C on electrode surface.
5. The diffusion impedance in corrosion process can evaluate the ion diffusion efficient in porosity of corrosion scales, and the calculating results show that the porosity of corrosion scales of the HSLA steel is smaller than the mild steel, indicating that the corrosion scales on HSLA steel show better protective ability than that on mild steel, in agreement with the EIS results.

References

1. Schino AD, Kenny AM (2002) J Mater Sci Lett 21:1631
2. Schino AD, Kenny AM (2003) J Mater Sci 38:4725
3. Reed-Hill RE (1979) Physical metallurgy principles, 2nd edn. Litton Educational, New York
4. Heuer JK, Stubbings JF (1998) Corrosion 54:566
5. Mora-Mendoza JL, Turgoose S (2002) Corros Sci 44:1223
6. Ueda M, Takabe H (1999) In: Proceedings of NACE Corrosion/1999, NACE, San Antonio, TX, paper no. 13
7. Zhang CL, Cai DY, Liao B, Zhao TC, Fan YC (2004) Mater Lett 58:1524
8. Zhao YT, Yang SW, Shang CJ, Wang XM, Liu W, He XL (2007) Mater Sci Eng A 455:700
9. Alves VA, Brett CMA (2002) Electrochim Acta 47:2081
10. Yang Q, Luo JL (2000) Electrochim Acta 45:3927
11. Martini EMA, Muller IL (2000) Corros Sci 42:443
12. Davies DH, Burstein GT (1980) Corrosion 36:416
13. Wang LP, Lin YM, Zeng ZX, Liu MN, Xue QJ, Hu LT, Zhang JY (2007) Electrochim Acta 52:4346
14. Badawy WA, Ismail KM, Fathi AM (2006) Electrochim Acta 51:4182
15. Macdonald JR, Johnson WB (1987) Impedance Spectroscopy. Wiley, New York
16. Rammelt U, Reinhard G (1990) Electrochim Acta 35:1045
17. Stoyanov Z (1990) Electrochim Acta 35:1493
18. Mora-Mendoza JL, Turgoose S (2002) Corrs Sci 44:1223
19. Li DY (2006) Mater Rec Soc Symp Proc 887:227
20. Li W, Li DY (2005) Appl Surf Sci 240:388
21. Wang LP, Zhang JY, Gao Y, Xue QJ, Hua LT, Xu T (2006) Scripta Mater 55:660
22. Liu L, Li Y, Wang FH (2008) Electrochim Acta 53:2641
23. Macák J, Sajdl P, Kučera P, Novotný R, Vošta J (2006) Electrochim Acta 51:3575
24. Za QX (2002) An introduction to electrode processes kinetics. Science Press, Beijing